Asian Journal of Applied Science and Technology (AJAST)
Volume 8, Issue 1, Pages 118-132, January-March 2024

Characterization of Reservoir Sands Using 3-D Seismic Attributes in FUBA Field, Onshore Niger Delta, Nigeria

U. Ochoma[1*], I. Tamunobereton-ari[2], A.R.C. Amakiri[3] & F.B. Sigalo[4]

[1-4]*Department of Physics, Rivers State University, P.M.B 5080, Port Harcourt, Nigeria.*
Corresponding Author (U. Ochoma) Email: umaocho@gmail.com[*]

DOI: https://doi.org/10.38177/ajast.2024.8110

Article Received: 13 January 2024 *Article Accepted: 21 March 2024* *Article Published: 28 March 2024*

ABSTRACT

Characterization of reservoir sands using 3D seismic attributes in Fuba Field, onshore Niger Delta, Nigeria are here presented. Well-log and 3D Seismic data were obtained from Shell Petroleum Development Company. Seismic interpretation was carried out using Petrel software. The structural interpretation of seismic data reveal highly synthetic and antithetic faults which are in line with faults trends identified in the Niger Delta. Two distinct horizons were mapped. Reservoir M is found at a shallower depth from 10937 to 10997 ft while reservoir N is found at a depth ranging from 11213 to 11241 ft respectively. Petrophysical summary of the sand units revealed that the area is characterized by high sand/shale ratio, effective porosity ranged from 16 to 37% and hydrocarbon saturation between 55 and 82%. By extracting attribute maps of variance, dip magnitude, average instantaneous frequency, average positive amplitude and RMS amplitude, characterization of the sand units in terms of reservoir geomorphological features, facies distribution and hydrocarbon potential was achieved. The variance values ranges from 0.0 to 1.0. The dip magnitude values ranges from 0 to 90 degrees. The Variance edge analysis and dip magnitude were used to delineate the prominent and subtle faults in the area. The average instantaneous frequency results indicate lower frequency range of 7 to 15 Hz at the center of the field indicating that this part comprises of substantially thick facies compared to its surroundings. The RMS amplitude values range from 0 to 13,000 in the reservoirs. The average positive amplitude and RMS attributes analysis indicate the presence of hydrocarbon in the seismic data. Results from this study have enhanced the delineation of drillable locations which are not recognized on conventional seismic interpretations, which could be further evaluated for hydrocarbon production.

Keywords: Reservoir sands; Dip magnitude; Average positive amplitude; Niger Delta; Nigeria.

1.0. Introduction

Reservoir characterization entails identifying, mapping and estimating petrophysical, structural, stratigraphic and geometric reservoir properties for effective development and exploitation of hydrocarbons from well and seismic data (Munyithya, et al., 2020). The description and evaluation of these subsurface features, in terms of structure, stratigraphy and reservoir properties, from conventional interpretation of seismic data is always challenging because of the complexity of the subsurface to seismic wave propagation (Chopra, and Marfurt, 2005; Nasser, 2020). Through seismic attribute analysis, these features on seismic data can be fully identified and evaluated by emphasizing on the individual component of the seismic wave in terms of the arrival time, frequency, amplitude and attenuation. Seismic attributes analysis involves the procedure used to extract corresponding subsurface geological information from seismic sections (Allstair, 2011). Subsurface quantitative interpretations require seismic attributes to supplement conventional seismic reflection amplitudes (Lefeuvre, and Wrolstad, 1995). Reservoir properties such as the geometry, sand thickness, sand/shale ratio, porosity, permeability, and water saturation define the accumulation and production of hydrocarbon in a field (Olaleye, et al., 2021). Seismic attributes are used in most seismic exploration and reservoir study to correctly image the subsurface geological structures, correctly characterize the amplitudes of the seismic data and to obtain information on reservoir properties (Pramanik, et al., 2002; Van, 2000; Vig, 2002). As such, seismic attributes analyze subsurface heterogeneity by describing its geomorphology (Chen, et al. 2020; Karbalaali, et al. 2018; Schneider, et al. 2016), facies changes (Chinwuko, et al. 2015; Wang, et al. 2017) and physical properties (Nawaz, et al. 2020) in terms of quality, quantity and aerial extent.

The application and efficiency of seismic attributes for stratigraphic features characterization is emphasized by the works of Jie et al. (2017), Othman et al. (2018) and Zhao et al. (2016). Jie et al. (2017) developed a workflow to improve the quality of coherence attributes. The skeletonized result rejects noise and enhances discontinuities seen in the vertical and lateral directions. The method was found to be better at tracking short faults and stratigraphic discontinuities. Zhao et al. (2016) preserved the distance in the input data space into the self-organizing maps (SOMs) latent space, which made the internal relation among data vectors on an SOM facies map better presented. This resulted in a more reliable classification. They were able to observe architectural elements that are over looked when using a conventional seismic amplitude volume for interpretation.

This study is taken from Fuba Field, Onshore, Niger Delta, Nigeria. The ultimate deliverable of this study was characterization of reservoir sands using 3D seismic attributes of the area. The major components of the study are: (a) Well Correlation performed in order to determine the continuity of the reservoir sand across the field. (b) Petrophysical evaluation. (c) Seismic Interpretation which involves well-to-seismic tie, fault mapping, horizon mapping, time surface generation and generation of seismic attributes. Seismic attributes were analyzed and reservoir properties predicted from the seismic attributes. This aids in giving more insight into characterization of reservoir sands using 3D seismic attributes.

2.0. Location and Geology of the Study Area

The proposed study area Fuba Field is located in the onshore Niger Delta region. Figure 1 the map of the Niger Delta region showing the location of the study area while Figure 2 shows the base map showing well locations in the study area. The Niger Delta lies between latitudes 4° N and 6° N and longitudes 3° E and 9° E (Whiteman, 1982). The Delta ranks as one of the major oil and gas provinces globally, with an estimated ultimate recovery of 40 billion barrels of oil and 40 trillion cubic feet of gas (Adegoke et al., 2017).

The coastal sedimentary basin of Nigeria has been the scene of three depositional cycles (Short and Stauble, 1967). The first began with a marine incursion in the middle Cretaceous and was terminated by a mild folding phase in Santonian time. The second included the growth of a proto-Niger delta during the Late Cretaceous and ended in a major Paleocene marine transgression. The third cycle, from Eocene to Recent, marked the continuous growth of the main Niger delta. A new threefold lithostratigraphic subdivision is introduced for the Niger delta subsurface, comprising an upper sandy Benin Formation, an intervening unit of alternating sandstone and shale named the Agbada Formation, and a lower shaly Akata Formation. These three units extend across the whole delta and each ranges in age from early Tertiary to Recent. They are related to the present outcrops and environments of deposition. A separate member of the Benin Formation is recognized in the Port Harcourt area. It is Miocene-Recent in age with a minimum thickness of more than 6,000ft (1829m) and made up of continental sands and sandstones (>90%) with few shale intercalations (Horsfall et al., 2017).

Subsurface structures are described as resulting from movement under the influence of gravity and their distribution is related to growth stages of the delta (Ochoma et al., 2020). Rollover anticlines in front of growth faults form the main objectives of oil exploration, the hydrocarbons being found in sandstone reservoirs of the Agbada Formation. The oil in geological structures in the basin may be trapped in dip closures or against a synthetic or antithetic fault.

Asian Journal of Applied Science and Technology (AJAST)
Volume 8, Issue 1, Pages 118-132, January-March 2024

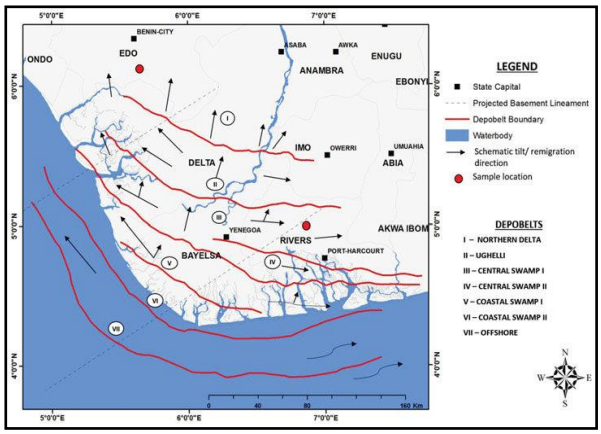

Figure 1. Map of Niger Delta Showing the study Area

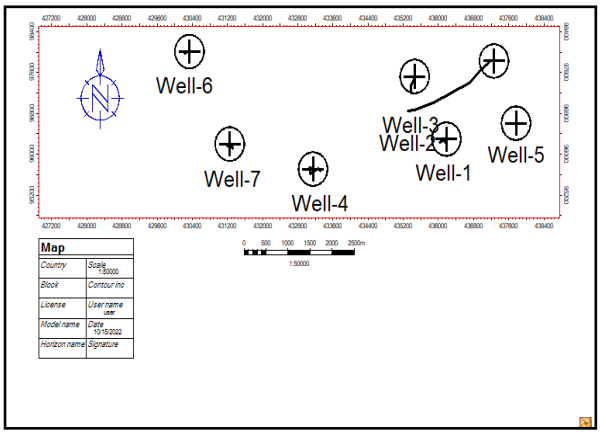

Figure 2. Base Map Showing Well Locations in the Study Area

3.0. Materials and Methods

3.1. Well-to-Seismic Ties

Well correlation is the first stage of the pre-interpretation process. The process of well correlation involves lithologic description, picking top and base of sand-bodies, fluid discrimination and then linking these properties from one well to another based on similarity in trends. In between these two lithologies in the subsurface, the gamma ray log is often used. Correlation of reservoir sands was achieved using the top and base of reservoir sands picked. The correlation process was possible based on similarity in the behavior of the gamma ray log the Niger Delta; the predominant lithologies are sands and shales. In order to discriminate shapes. Also, the thickness of the shale bodies overlying and underlying the sand body is considered during Correlation. After defining the lithologies, the resistivity log was used for discriminating the type of fluid occurring within the pores in the rocks.

There are five basic steps involved in seismic interpretation relevant to this study and they include; Well-to-seismic ties, Fault Mapping, Horizon mapping, Time surface generation and Attributes generation. Well-to-seismic tie is a process that enables the visualization of well information on seismic data. For this process to be achieved, the following are basic requirements; checkshot, sonic log, density log and a wavelet. The sonic log, which is the reciprocal of velocity, was calibrated using the checkshot data. The calibration process is necessary in order to improve the quality of the sonic log because the sonic log is prone to washouts and other wellbore related issues. The results of calibrating the sonic log with the checkshot gives a new log called the calibrated sonic log.

The calibrated sonic log is used along with the density log to generate an acoustic impedance (AI) log. The acoustic impedance log is calculated for each layer of rock. The next step involves generating the reflectivity coefficient (RC) log. The RC is calculated and generated using the AI log. The RC log generated is then convolved with a wavelet to generate a synthetic seismogram which is comparable with the seismic data. The extended white 2 wavelet utilized for convolution is extracted from the seismic data. The synthetic seismogram was generated for every well that had checkshot, density and sonic log. The reflections on the synthetic seismogram were matched with the reflections on seismic data. The mathematical expressions that govern the entire well-to-seismic tie workflow are presented below:

$$AI = \rho v \quad (1)$$

$$RC = \frac{\rho_2 v_2 - \rho_1 v_1}{\rho_2 v_2 + \rho_1 v_1} \quad (2)$$

$$\text{Synthetic Seismogram} = \frac{\rho_2 v_2 - \rho_1 v_1}{\rho_2 v_2 + \rho_1 v_1} * wavelet \quad (3)$$

where AI = acoustic impedance, RC = reflection coefficient, ρ = density; v = velocity.

Faults were identified as discontinuities or breaks in the seismic reflections. Faults were mapped on both inline and cross-line directions. Horizons are continuous lateral reflection events that are truncated by fault lines. The horizon interpretation process was conducted along both inline and crossline direction. At the end of the horizon mapping, a seed grid is generated which serves as an input for time surface generation. Time surfaces were generated using the seed grids gotten from the horizon mapping process.

3.2. Petrophysical evaluation

Petrophysical evaluation was carried out using empirical correlations to estimate the petrophysical parameters of the reservoirs. Correlations established between the desired rock properties and measured physical properties were used to derive rock properties such as shale volume (V_{sh}), effective porosity (ϕ_E) and water saturation (S_w).

3.2.1. Shale Volume (V_{sh})

This is the space occupied by shale or the fraction of shale (clay), present in reservoir rock (Cannon, 2018). The volume of shale is determined from mathematical correlations and gamma ray index. In mathematical equations, the volume of shale is represented as V_{sh}. The gamma ray index (GR_{index}) was first calculated in order to calculate the shale volume based on Schlumberger (1974) empirical equation as follows;

$$\text{GR}_{\text{index}} = \frac{GR_{log} - GR_{min}}{GR_{max} - GR_{min}} \quad (4)$$

Where;

$GR_{log} = GR\ log\ reading\ of\ formation$, $GR_{min} = GR\ sand\ baseline$ and

$GR_{max} = GR\ shale\ baseline$

The Larionov (1969) equation for tertiary reservoirs was utilized for calculating the shale volume as follows;

$$\text{Vsh} = 0.083 \times (2^{(3.7 \times GR_{index})} - 1) \quad (5)$$

3.2.2. Effective Porosity

The effective porosity is the porosity that is responsible for flow to occur within the reservoir. Effective porosity (ϕ_E) was calculated using volume of shale (V_{sh}) and total porosity (ϕ_T) as follows (Dresser, 1979);

$$\emptyset_E = (1 - Vsh) \times \emptyset_T \quad (6)$$

Where;

$\emptyset_E = Effective\ porosity$, $\emptyset_T = Total\ Porosity$ and $Vsh = Volume\ of\ shale$.

3.2.3. Water Saturation

This is the relative extent to which the pores in rocks are filled with water. Saturation is expressed as the fraction, or percent, of the total pore volume occupied by the oil, gas, or water. Water saturation is denoted as S_w and is expresses in percent or fraction. Water saturation is predominantly controlled by porosity and formation resistivity. It was calculated using Archie (1942) empirical model as follows;

$$S_w = \left(\frac{a \times R_w}{R_t \times \emptyset_t^m}\right)^{1/n} \quad (7)$$

Where;

S_w = Archie's water saturation for clean sand, a = tortuosity factor = 1

m = cementation exponent = 2, n = saturation exponent = 2

R_t = formation resistivity (read from log), R_w = formation water resistivity (read from log) and ϕ_t = total porosity.

3.3. Seismic Attributes

Among the seismic attributes that have been used in the visualization of the geology of the subsurface are variance, dip magnitude, average instantaneous frequency, instantaneous positive amplitude and root mean square amplitude. The variance and dip magnitude analysis were applied to the seismic inline 8515 while the average instantaneous frequency, instantaneous positive amplitude and root mean square amplitude were generated as surface attributes.

3.3.1. Variance (Edge Detection) Method

In the Petrel software, the variance attribute uses an algorithm that computes the local variance of the seismic data through a multi-trace window with user-defined size. The local variance is computed from horizontal sub-slices for each voxel. A vertical window was used for smoothing the computed variance and the observed amplitude normalized. The variance attribute measures the horizontal continuity of the amplitude that is the amplitude difference of the individual traces from their mean value within a gliding CMP window.

$$\sigma^2 = \frac{1}{n}\sum_{f_i=1}^{n}(x_i + x_m)^2 \quad (8)$$

Where σ = standard deviation, σ^2 = variance, n = the number of observations, f_i = frequency

x_i = the variable, x_m = mean of x_i.

3.3.2. Dip magnitude

Dip magnitude is analogous to strike and dip of sedimentary layers. The dip magnitude is defined as the angle between the steepest direction of a plane and a horizontal plane, where values range from 0 to 90. The dip magnitude attribute computation in Petrel software makes use of the inbuilt formula:

$$\text{True dip} = \tan^{-1}\left(\frac{\tan(\theta_y)}{\tan(\beta_x)}\right) \quad (9)$$

where $\theta_y =$ apparent dip in a direction (y) and $\beta_x =$ dip azimuth relative to a direction (x).

Dip magnitude is a good attribute, not only for showing overall structure folds, but can be used to identify faults with very small displacement.

3.3.3. Determination of Average Instantaneous Frequency

Instantaneous frequency is a temporal rate of change of instantaneous phase. It is the sinusoid frequency in a short window that fits the seismic trace around the corresponding time. It also estimates the average. Given an analytic signal representation, instantaneous frequency is well defined as the time derivative of phase:

$$f(t) = \frac{d\phi(t)}{dt} \quad (10)$$

where $f(t) =$ instantaneous frequency, with angle $\phi =$ in radians and time (t) in seconds, this results in the results of instantaneous frequency in units of radians/seconds. Dividing equation 10 by 2π gives the unit in Hertz (Hz).

3.3.4. Determination of Average Instantaneous Amplitude

The instantaneous amplitude measures reflectivity strength, which is proportional to the square root of the total energy of the seismic signal at an instant time. The amplitude is the distance between the centerline and the peak or trough. It is given by

$$x = A\sin(\omega t + \phi) \quad (11)$$

or

$$x = A\cos(\omega t + \phi) \quad (12)$$

where $x =$ displacement of the wave (meter), $A =$ amplitude , $\omega =$ angular frequency (radians/seconds), $t =$ time period and $\phi =$ phase angle. The amplitude formula is also expressed as the average of the sine or cosine functions maximum and minimum values. The absolute value of the amplitude was used.

3.3.5. Determination of Root Mean Square (RMS) Amplitude

Root mean square (RMS) amplitude is used to obtain a scaled estimate of seismic trace envelope. It is obtained in the software by sliding a tapered window of N samples as the square root of the sum of all the trace value x squared. The RMS attribute computation in Petrel software makes use of the inbuilt formula:

$$X_{rms} = \sqrt{\frac{1}{N}\sum_{n=1}^{N} w_n x_n^2} \quad (13)$$

where $X_{rms} =$ root mean square amplitude, $w_n =$ window values, $N =$ number of samples in the window, $x =$ trace value.

Asian Journal of Applied Science and Technology (AJAST)
Volume 8, Issue 1, Pages 118-132, January-March 2024

4.0. Results and Discussion

4.1. Reservoir Identification and Correlation

The results for lithology and reservoir identification are presented in (Figure 3). A total of four sand bodies (L, M, N and O) were identified and correlated across all seven wells in the field. Two reservoir sands were selected for the purpose of this study (M and N). The resistivity logs which reveals the presence of hydrocarbons were used to identify the hydrocarbon bearing sands. On Figure 3, the sands are coloured yellow while shales are grey in colour.

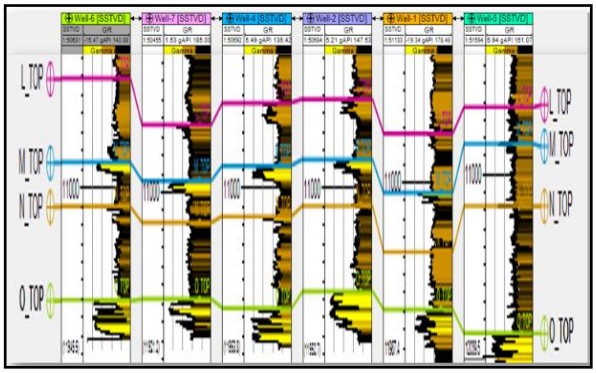

Figure 3. Well section showing reservoir identified and correlated across Fuba Field

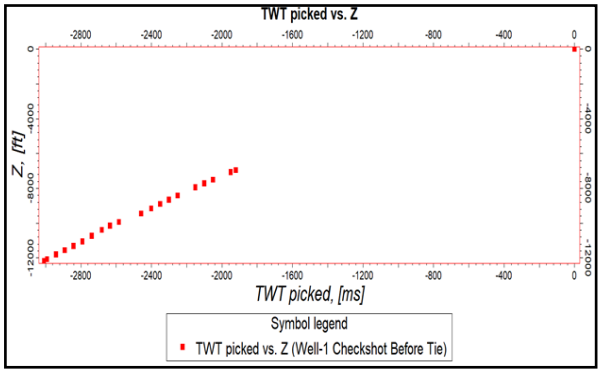

Figure 4. Checkshot Quality for Well-1

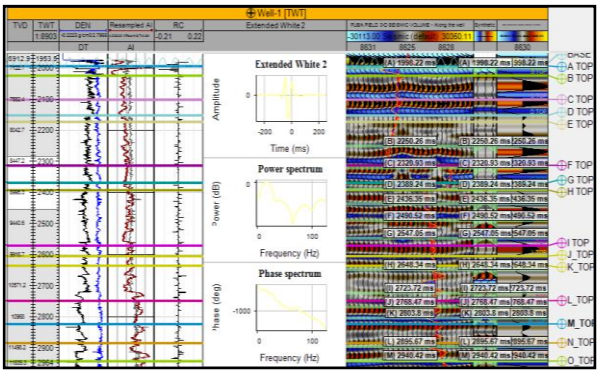

Figure 5. Synthetic seismogram generation and well-to-seismic tie conducted for Fuba Field using Well-1 Checkshot

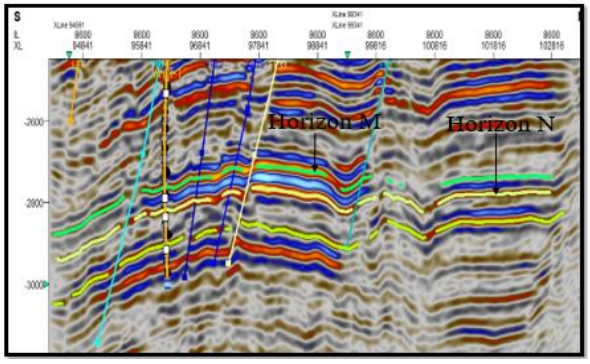

Figure 6. Faults and horizons interpreted along seismic inline section

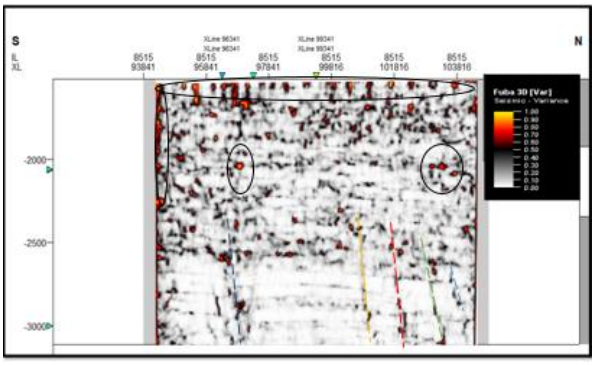

Figure 7. Variance edge inline 8515

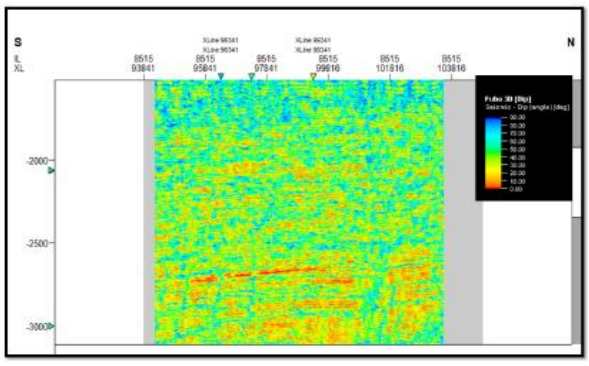

Figure 8. Dip Magnitude inline 8515

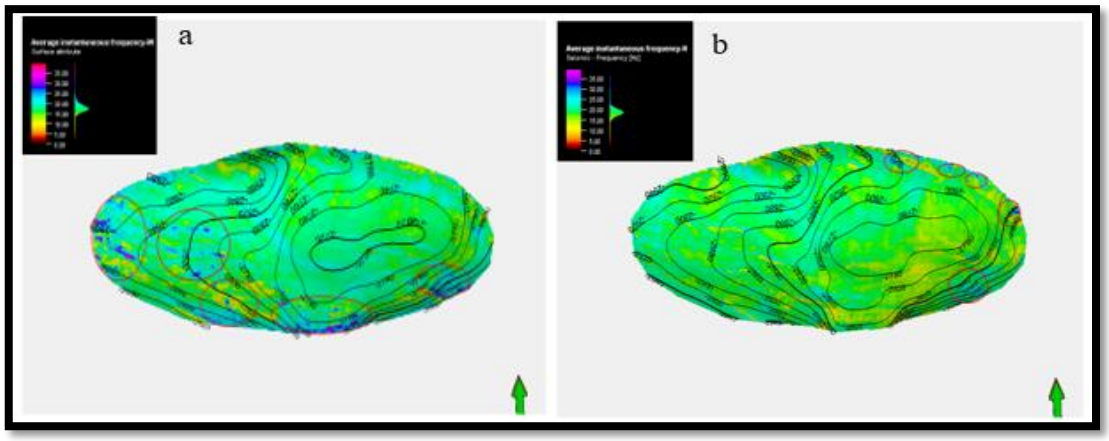

Figure 9. Average Instantaneous Frequency Maps for Reservoir Surfaces (a) Reservoir Surfaces M, (b) Reservoir Surfaces N

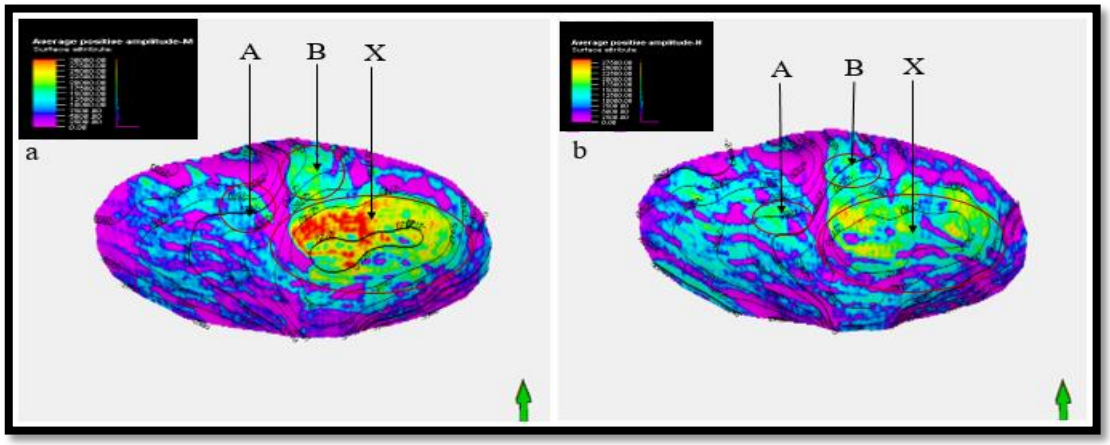

Figure 10. Instantaneous Positive Amplitude Maps for Reservoir Surfaces

Instantaneous Positive Amplitude Map Showing Identified Hydrocarbon Leads (A and B) away from the Producing Zone "X" for Reservoir Surface M (b) Instantaneous Positive Amplitude Map Showing Identified Hydrocarbon Leads (A and B) away from the Producing Zone "X" for Reservoir Surface N

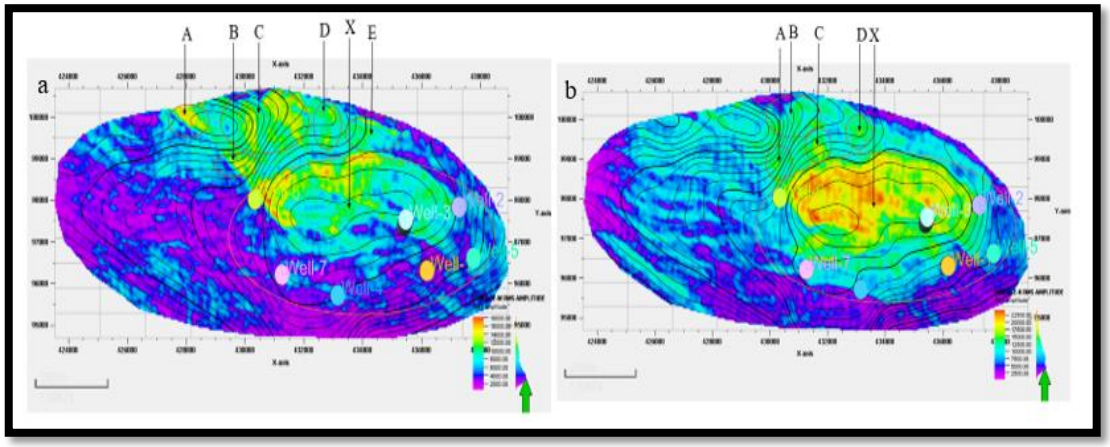

Figure 11. RMS Amplitude Maps for Reservoir Surfaces

(a) RMS Amplitude Map Showing Identified Hydrocarbon Leads (A, B, C, D and E) away from the Producing Zone "X" for Reservoir Surface M (b) RMS Amplitude Map Showing Identified Hydrocarbon Leads (A, B, C and D) away from the Producing Zone "X" for Reservoir Surface N

4.2. Well-to-seismic Tie

The checkshot quality for Well-1 utilized for well-to-seismic tie is shown in Figure 4. The results for well-to-seismic tie conducted on Fuba field using density log, sonic log and checkshot of Well-1 is presented in Figure 5. An extended white 2 wavelet was used to give a near perfect match between the seismic and synthetic seismogram.

4.3. Fault and Horizon Interpretation

The results for the interpreted faults in Fuba field are presented in Figure 6 shows both synthetic and antithetic faults interpreted along seismic inlines. Faults are more visible along the inline direction because this direction reveals the true dip position of geologic structures. The variance time slice was used to validate the interpreted faults. All interpreted faults are normal synthetic and antithetic faults. A total of thirty-six faults were interpreted across the entire seismic data. Of the 36 interpreted faults, only F1 (synthetic fault) and F4 (antithetic fault) faults are regional, running from the top to bottom across the field. Hence, these faults play significant roles in trap formation at the upper, middle and lower sections of the field.

The results for the interpreted seismic horizons (Horizons M and N) are also presented in Figure 6. On these horizons, the fault polygons were generated and eliminated. The horizons were used as inputs for the generation of reservoir time surfaces.

4.4. Petrophysical Evaluation

The results of petrophysical evaluation for the reservoir (M and N) are presented in Tables 1 and 2. From the tables, it was deduced that shale volume (V_{sh}) ranges from 9.00 to 11.00% with an average of 9.14% and 10.28% in reservoir sands M and N. Effective porosity of the sand units range from 17.00 to 23.00% with an average of 20.30% and 19.30%. Rider (1986) classified reservoirs having porosity ranging between 20 to 30% as very good quality reservoirs. Based on this classification, reservoir M and N are classed as very good quality. The reservoir sands have moderate water saturation resulting in high hydrocarbon saturation values (62% and 52%).

4.5. Seismic Attributes

A series of seismic volume attributes such as variance edge, dip magnitude, average instantaneous frequency, average positive amplitude and Root Mean Square (RMS) amplitude were generated in Petrel software interface for characterization of reservoir sands within the study area.

Figure 7 shows the computed variance attributes of the seismic section. The variance values range from 0.0 to 1.0. Values of variance equal to 1 represent discontinuities while a continuous seismic event is represented by the value of 0. The high values are denoted with red to yellow colorations. On the variance map, the areas dotted with blue, green, orange and pink colored lines signify values that correspond to the location of the discontinuity. The discontinuities may be interpreted as faults and boundaries as shown by the lines drawn on the variance attribute map (Law, and Chung, 2006). The variance edge enhanced the faults or sedimentological bodies within the seismic data volume. Furthermore, several bright spots are also delineated (in black circles and black ovals) which indicate high reflectivity sediments compared to their surroundings. These bright spots are an indication that a potential

hydrocarbon trap might exist in the area. The darkest regions in the seismic section, which make vertical stripes, may be interpreted as faults or fractures. The zones with low variance values are due to similar seismic traces. Areas with red patches represent lineaments/discontinuities while grey areas represent the structural framework of the field.

The variance attribute is edge imaging and detection techniques. It is used for imaging discontinuity related to faulting or stratigraphy in seismic data. Variance attribute is proven to help in imaging of channels, fault zones, fractures, unconformities and the major sequence boundaries (Pigott, et al., 2013).

Figure 8 shows the dip magnitude of the faults. The dip magnitude values range from 0 to 90. On Figure 8, the green colors represent areas of greater dip, while the red colors represent areas of shallower dip.

Figure 9 shows the average instantaneous frequency maps for the studied reservoir surfaces (reservoir surface M and N). Average instantaneous frequency is generally used for facies distribution (Liyuan, et al., 2019). This was possible because average instantaneous frequency represents the average frequency of the amplitude spectrum of seismic wavelet. An increase in density of a medium due to the presence of shale in a reservoir increases its average instantaneous frequency hence analyzing shale/sand distribution. Likewise, at higher frequencies, there is always an increase in the vertical resolution and as such, highlighting thin reservoir layers. Thickness decreases with increase in instantaneous frequency (Ogiesoba, et al., 2018). Observations on Figure 9a show that the western, southern and southeast parts consist of sands with more volume of shale and increased instantaneous frequency (indicated by areas in red circles). Also, facies distribution in the area revealed irregular thickness of the reservoir down to the southern part.

A significant feature was observed at the northeastern and southeastern part of Figure 9b from the sharp frequency increase, indicating sudden change in facies in terms of thickness and sand percentage (indicated by areas in red circles). This sharp frequency increase is an indication of stratigraphic play around the area. The characteristic frequency increase at this part of the field distinctively analyzes the thickness and the amount of shale in the stratigraphic body.

Observations on Figures 9a and 9b shows that the center of the field was mapped by lower frequency range 7 to 15 Hz, indicating that this part comprises of substantially thick facies compared to its surroundings. This was interpreted as decrease in the amount of shale in the sand body with decrease frequency and it was confirmed by the V_{sh} interpretation of the penetrated sand bodies (Tables 1 and 2). It was also observed that the thickness at the center of the field is controlled by the bounding growth faults.

Figure 10 gives the hydrocarbon potentials of the delineated geologic features using average positive amplitude attribute. This was done by analyzing the amplitude changes and relating them to possible change in subsurface porosity within the sand units. Average positive amplitude attribute measures reflectivity of seismic events, as such, high porosity is inferred at high reflectivity (also referred to as bright spots). Figure 10 reveals two main characteristic display of high and low amplitude areas, indicating high and low porosity respectively. Along the western part of the field (Figures 10a and 10b), bright amplitude anomalies (A and B) were observed. The bright amplitude anomalies are reflection surface resulting from matrix fluid contact on the surface of the sand unit. All the

wells penetrated through these reservoirs at the point under well control (X) have high porosity between 17 and 23% and water saturation between 34 and 60% (Tables 1 and 2). These two high reflectivity anomalies (A and B) with high average positive amplitude identified on Figures 10a and 10b could serve as hydrocarbon prospects for hydrocarbon exploitation.

The RMS amplitude was generated for the two studied reservoir surfaces (reservoir surface M and N). Figures 11a and 11b show the RMS amplitude maps. The RMS amplitude values range from 0 (purple) to 13,000 (red) in reservoir M and 0 (purple) to 12,000 (red) in reservoir N. The red-yellowish color represents hydrocarbon sands. Some of these hydrocarbon sands were not detected in the original seismic section. The observed changes may be due to changes in lithology or fluid content. RMS amplitude is similar to reflection strength and it is used in seismic exploration for delineating bright spots and amplitude anomalies (Fozao, et al., 2018; Omoja, and Obiekezie, 2019; Opara, and Osaki, 2018). It measures the acoustic intensity of a seismic wave. In a less dense medium, the intensity is expected to be high compared to a dense medium. Since the amplitude of the wave determines its intensity, this attribute was used to compliment the instantaneous amplitude attributes as high RMS attribute indicates spatial correlation to porosity and potential hydrocarbon reservoirs. High magnitude reflection strength are observed as prospects A, B, C, D and E in Figures 11a and 11b. The prospect zone B and C observed on Figure 11a and A and C observed on Figure 11b coincide with the previously identified stratigraphic features on Figures 10a and 10b. This confirms the possibility of the prospects for hydrocarbon exploitation. The high amplitude in the seismic data conforms to the structures and confirm the presence of hydrocarbon (Ajisafe, and Ako, 2013). The high amplitude ranges from light blue to yellow and red coloration. Root mean square amplitude is used as a good indicator of the presence of hydrocarbon in seismic data. The wells are located on this high-amplitude anomalies in each RMS attribute map.

Since both figures measure the seismic reflectivity of the subsurface, the higher the amplitude, the higher the porosity and the better the hydrocarbon productivity of the reservoir unit. From the stratigraphic geometry of the hydrocarbon prospect (Figure 11), the depositional process/stratigraphic deposits were identified on the basis of reflection termination and lateral changes in seismic reflection amplitudes. The RMS amplitude is used for identifying coarser-grained facies, compaction related effects and unconformities.

Table 1. Results of Petrophysical Evaluation for Reservoir Surface M

Wells	Reservoir Top (SSTV ft)	Reservoir Base (SSTV ft)	Net thickness (ft)	Shale Volume (%)	Effective Porosity (%)	Water Saturation (%)
Well-1	11054.00	11116.00	45.00	9.00	18.00	34.00
Well-2	10846.00	10894.00	48.00	9.00	21.00	36.00
Well-3	11154.00	11230.00	76.00	10.00	23.00	39.00
Well-4	10880.00	10967.00	87.00	9.00	23.00	34.00
Well-5	10830.00	10840.00	10.00	9.00	19.00	40.00
Well-6	10861.00	10919.00	58.00	9.00	19.00	39.00
Well-7	10936.00	11018.00	82.00	9.00	19.00	41.00
Average	10,937.29	10,997.71	58.00	9.14	20.30	38.00

Table 2. Results of Petrophysical Evaluation for Reservoir N

Wells	Reservoir Top (MD ft)	Reservoir Base (MD ft)	Net thickness (ft)	Shale Volume (%)	Effective Porosity (%)	Water Saturation (%)
Well-1	11376.00	11390.00	14.00	10.00	17.00	33.00
Well-2	11095.00	11111.00	16.00	10.00	20.00	51.00
Well-3	11440.00	11517.00	77.00	11.00	22.00	58.00
Well-4	11154.00	11182.00	28.00	10.00	22.00	32.00
Well-5	11172.00	11186.00	14.00	11.00	18.00	54.00
Well-6	11099.00	11125.00	26.00	10.00	18.00	45.00
Well-7	11161.00	11179.00	18.00	10.00	18.00	60.00
Average	11,213.71	11,241.42	28.00	10.28	19.30	48.00

5.0. Conclusion

A total of four sand bodies (L, M, N and O) were identified and correlated across all seven wells in the field. All interpreted faults are normal synthetic and antithetic faults. A total of thirty-six faults were interpreted across the entire seismic data. Of the 36 interpreted faults, only F1 (synthetic fault) and F4 (antithetic fault) faults are regional, running from the top to bottom across the field. Hence, these faults play significant roles in trap formation at the upper, middle and lower sections of the field. Two horizons (M and N) were selected for the study. The seismic attributes interpreted include variance, dip magnitude, average instantaneous frequency, average positive amplitude and root mean square amplitude. The variance values ranged from 0.00 to 1.00. The dip magnitude values ranged from 0 to 90 degrees. The variance and dip magnitude revealed the subtle structures and faults in the seismic section. The average instantaneous frequency results indicate lower frequency range of 7 to 15 Hz at the center of the field indicating that this part comprises of substantially thick facies compared to its surroundings and the thickness in this part is controlled by the bounding growth faults. The RMS amplitude values range from 0 to 13,000 in the reservoirs. The average positive amplitude and RMS attributes maps generated for reservoir tops of interest were seen to have a similar pattern of bright spot anomaly. These amplitude anomalies served as direct hydrocarbon indicators (DHIs), unravelling the presence and possible hydrocarbon prospective zones. Also, it indicates that away from the producing zone that there exist other hydrocarbon prospective zones which show good trapping structures such as anticlines which support hydrocarbon accumulation. The structural high part on Figures 9 and 10 are considered viable prospects A, B, C, D and E respectively as they are attributed with low shale volume, moderate sand thickness and high porosity anomaly. Seismic attributes analysis has demonstrated that this technique can be used effectively to understand the sand thicknesses, lateral facies distribution and a better delineation of hydrocarbon potential in the study area. The interpretation and assessment of the field revealed that the most exploitable hydrocarbon prospect area is in the northwestern, northeastern and central parts based on the efficient reservoir qualities in terms of low shale/sand ratio, good sand thickness, high porosity, and efficient hydrocarbon saturation, as interpreted from seismic attributes transforms of the field. However, further work is recommended to be concentrated on the identified exploitable part of the field with the intention to upgrade the area into drillable prospect by estimating its reserve. Therefore, to effectively evaluate the prospects, geostatistics is required to predict reservoirs properties from areas under well control to the prospect areas.

Declarations

Source of Funding

The study has not received any funds from any organization.

Competing Interests Statement

The authors have declared no competing interests.

Consent for Publication

The authors declare that they consented to the publication of this study.

Authors' Contributions

All the authors took part in literature review, research, and manuscript writing equally.

Acknowledgements

The authors are grateful to Shell Petroleum Development Company of Nigeria (SPDC), Port Harcourt Nigeria for the release of the academic data for the purpose of this study.

References

[1] Munyithya, M., Ehirim, N.C., Dagogo T., & K'orowe, M.O. (2020). Seismic Amplitudes and Spectral Attribute Analysis in Reservoir Characterisation, 'MUN' Onshore Niger Delta Field. Journal of Petroleum Exploration and Production Technology, 10: 2257–2267.

[2] Chopra, S., & Marfurt, K.J. (2005). Seismic Attributes—a Historical Perspective. Geophysics, 70(5): 3–28.

[3] Naseer, M.T. (2020). Seismic Attributes and Reservoir Simulation Applications to Image the Shallow-Marine Reservoirs of Middle Carbonals SW Pakistan. Journal of Petroleum Science and Engineering, 195: 10771–107711.

[4] Allstair, R.B. (2011). Interpretation of 3D Seismic Data, 7th Edition. The American Association of Petroleum Geologists and Society of Exploration Geophysics, Tulsa.

[5] Lefeuvre, F.E., Wrolstad, K.H., Zou, K.S., Smith, L.J., Maret, J.P., & Nyein, U.K. (1995). Sand-Shale Ratio and Sandy Reservoir Properties Estimation from Seismic Attributes: An Integrated Study. Society of Exploration Geophysics Expanded Abstracts, 95: 108–110.

[6] Olaleye, K.O., Enikanselu, A.P., & Ayuk, A.M. (2021). Characterization of Reservoir Sands Using 3D Seismic Attributes in The Coastal Swamp Area of Niger Delta Basin. Journal of Petroleum Exploration and Production Technology, 11: 3995–4004.

[7] Pramanik, A.G., Singh, V., Srivastava, A.K., & Katiyar, R. (2002). Stratigraphic Inversion for Enhancing Vertical Resolution. Geohorizons, 7(2): 8–18.

[8] Van, R.P. (2000). The Past, Present, and Future of Quantitative Reservoir Characterization. Leading Edge, 19(8): 878–881.

[9] Vig, R., Singh, V., Kharoo, H.L., Tiwari, D.N., Verma, R.P., Chandra, M., & Sen, G. (2002). Post Stack Seismic Inversion for Delineating Thin Reservoirs: A Case Study. Mumbai, 4th conference and Exposition in Petroleum Geophysics, Pages 287–291.

[10] Chen, H., Zhu, X., Shi, R., & Zhang, Z. (2020). Seismic Geomorphology of Shoal-Water Deltaic and Mixed Carbonate-Siliciclastic Beach-Bar Systems in Hanging Wall of Rift Basins: Paleogene of the Raoyang Sag Bohai Bay Basin, China. Interpretation, 8: 1–19.

[11] Karbalaali, H., deGroot, P., Javaherian, A., Qayyum, F., Dahlke, S., & Torabi, S. (2018). Identification of Shallow Geoharzard Channels Based On Discontinuity Seismic Attributes in The South Caspian Sea. Geophysics, 83(6): 317–322.

[12] Schneider, S., Eichkitz, C.G., Schreilechner, M.G., & Davis, J.C. (2016). Interpretation of Fractured Zones Using Seismic Attributes-Case Study from Teapot Dome, Wyoming USA. Interpretation, 4(2): 249– 260.

[13] Chinwuko, A.I., Onwuemesi, A.G., Anakwuba, E.K., Onyekwelu, C.U., Okeke, H.C., & Obiadi, I.I. (2015). Coblending of Seismic Attributes for Interpretation of Channel Geometries in Rence Field of Niger Delta Nigeria. Interpretation, 3(4): 183–195.

[14] Wang, X., Zhang, B., Zhao, T., Hang, J.W.O.H., & Yong, Z. (2017). Facies Analysis by Integrating 3D Seismic Attributes and Well Logs for Prospect Identification and Evaluation-A Case Study from Northwest China. Interpretation, 5(2): 61–74.

[15] Nawaz, M.A., Curtis, A., Shahraeeni, S., & Gerea, C. (2020). Variational Bayesian Inversion of Seismic Attributes Jointly for Geologic Facies and Petrophysical Rock Properties. Geophysics, 85(4): 1–18.

[16] Jie, Q., Machado, G., & Marfurt, K. (2017). A Workflow to Skeletonized Faults and Stratigraphic Features. Geophysics, 82(4): 57–70.

[17] Othman, A.A., Fatty, M., & Negm, A. (2018). Identification of Channel Geometries Applying Seismic Attributes and Spectral Decomposition Technique, Temsah Field, offshore East Nile Delta, Egypt. NRIAG Journal of Astronomy and Geophysics, 7(1): 52–61.

[18] Zhao, T., Zhang, J., Li, F., & Marfurt, K.J. (2016) Characterizing Turbidite System in Canterbury Basin, New Zealand Using Seismic Attributes and Distance Preserving Self-Organizing Maps. Interpretation, 4(1): 79–89.

[19] Whiteman, A. (1982). Nigeria: Its Petroleum Ecology Resources and Potential. London, Graham and Trotman.

[20] Adegoke, O.S., Oyebamiji, A.S., Edet, J.J., Osterloff, P.L., & Ulu, O.K. (2017). Cenozoic Foraminifera and Calcareous Nannofossil Biostratigraphy of the Niger Delta. Elsevier, Cathleen Sether, United States.

[21] Short, K.C., & Stable A.J. (1967). Outline of Geology of Niger Delta. Bulletin of America Association of Petroleum Geologists, 51(5): 761–779.

[22] Horsfall, O.I., Uko, E.D., Tamunoberetonari I. & Omubo-Pepple, V.B. (2017). Rock-Physics and Seismic-Inversion Based Reservoir Characterization of AKOS FIELD, Coastal Swamp Depobelt, Niger Delta, Nigeria. IOSR Journal of Applied Geology and Geophysics, 5(4): 59–67.

[23] Ochoma, U., Uko E.D., & Horsfall, O.I. (2020). Deterministic Hydrocarbon Volume Estimation of the Onshore Fuba Field, Niger Delta, Nigeria. IOSR Journal of Applied Geology and Geophysics, 8(1): 34–40.

[24] Cannon, S. (2018). Reservoir Modelling: A Practical Guide. John Wiley and Sons, Inc., 111 River Street, Hoboken, NJ 07030, USA.

[25] Schlumberger (2007). Interpreter's Guide to Seismic Attributes.

[26] Larionov, V. (1969). Borehole Radiometry. Moscow, U.S.S.R., Nedra.

[27] Dresser, A. (1979). Log Interpretation Charts, Dresser Industries Inc., Houston, Texas: 107.

[28] Archie, G.E. (1942). The Electrical Resistivity Log as an Aid in Determining Some Reservoir Characteristics. Journal of Petroleum Technology, 5: 54–62.

[29] Rider, M.H. (1986). The Geological Interpretation of Well Logs. John Wiley and sons, Inc., New York.

[30] Law W.K., & Chung A.S.C. (2006). Minimal Weighted Local Variance as Edge Detector for Active Contour Models. In Narayanan et al. PJ (eds.), Accv 2006, LNCS – 3851: 622–632.

[31] Pigott, J.D., Kang, M.I.H., & Han, H.C. (2013). First Order Seismic Attributes for Clastic Seismic Facies Interpretation: Examples from the East China Sea. Journal of Asian Earth Science, 66: 34–54.

[32] Liyuan, X., Aarre, V., Barnes, A.E., Theoharis, T., Salman, N., & Tjaland, E. (2019). Seismic Attributes Benchmarking on Instantaneous Frequency. Geophysics, 84(3): 63–72.

[33] Ogiesoba, O.C., Ambrose, W.A., & Loucks, R.C. (2019). Investigation of Seismic Attributes, Depositional Environment and Hydrocarbon Sweetspot Distribution in The Serbian Field, Tarlor Formation, Southeast Texas. Interpretation 7(1): 49–66.

[34] Fozao, K.F., Fotso, L., Djieto-Lordon, A., & Mbeleg, M. (2018). Hydrocarbon Inventory of the Eastern Part of the Rio Del Rey Basin Using Seismic Attributes. J of Petroleum Exploration & Production Tech., 8: 655–665.

[35] Omoja U.C., & Obiekezie T.N. (2019). Application of 3D Seismic Attribute Analyses for Hydrocarbon Prospectivity in Uzot-Field, Onshore Niger Delta Basin, Nigeria. International Journal of Geophysics, Pages 1–11.

[36] Opara, A.I., & Osaki, L.J. (2018). 3-D Seismic Attribute Analysis for Enhanced Prospect Definition of "Opu Field'', Coastal Swamp Depo Belt Niger Delta, Nigeria. Journal of Applied Science, 18: 86–102.

[37] Ajisafe, Y.C., & Ako, B.D. (2013). 3-D Seismic Attributes for Reservoir Characterization of 'Y' field, Niger Delta, Nigeria. IOSR Journal of Applied Geology and Geophysics, 1: 23–31.